Inorganic Chemistry

Article

pubs.acs.org/IC

Redox Routes to Substitution of Aluminum(III): Synthesis and Characterization of $(IP^-)_2AlX$ (IP = α-iminopyridine, X = Cl, Me, SMe, S_2CNMe_2, C≡CPh, N_3, SPh, NHPh)

Thomas W. Myers, Alexandra L. Holmes, and Louise A. Berben*

Department of Chemistry, University of California, Davis, California 95616, United States

Supporting Information

ABSTRACT: Redox active ligands are shown to facilitate a variety of group transfer reactions at redox inert aluminum(III). Disulfides can be used as a two-electron group transfer reagent, and we show that $(IP^-)_2AlSR$ can be formed by reaction of $[(THF)_6Na][(IP^{2-})_2Al]$ (**1c**) with disulfides RSSR (where X = $C(S)NMe_2$, **4**; SMe, **5**). In a more general redox route to substitution of aluminum bis(iminopyridine) complexes, we report zinc(II) salts as a group transfer reagent. Reaction of $[(^RIP^{2-})_2Al]^-$ (R = H, **1c**; Me, **1d**) with ZnX_2 affords $(^RIP^-)_2AlX$ (where IP = iminopyridine, R = H, and X = Cl, **2**; CCPh, **6**; N_3, **7**; SPh, **8**; or R = Me and X = NHPh, **9**). Single crystal X-ray diffraction analysis of the complexes reveal that each of the five coordinate complexes reported here has a trigonal bipyramidal geometry with τ = 0.668 − 0.858. We observed a correlation between the greatest deviations from ideal trigonal bipyramidal symmetry (lowest τ values), the bond lengths consistent with smallest degree of ligand reduction, and the least polarizable X ligand in $(IP^-)_2AlX$. Complex **4** is six-coordinate and is best described as distorted octahedral. Variable temperature magnetic susceptibility measurements indicate that each of the complexes **3**−**9** has a biradical electronic structure similar to previously reported **2**. Magnetic exchange coupling constants in the range J = −94 to −212 cm^{-1} were fit to the data for **2**−**9** to describe the energy of antiferromagnetic interaction between ligand radicals assuming a spin Hamiltonian of the form $\hat{H} = -2J\hat{S}_{L(1)}\cdot\hat{S}_{L(2)}$. The strongest coupling occurs when the angle between the ligand planes is smallest, presumably to afford good overlap with the Al−X σ* orbital. Electrochemical properties of the complexes were probed using cyclic voltammetry and each of **3**−**9** displayed a reversible two-electron reduction and two quasi-reversible one-electron oxidation processes. The energy of the ligand based redox processes for **2**−**9** differ by about 150 mV over all complexes and show a correlation with the degree of IP^- reduction observed crystallographically; more reduced IP^- ligands require higher potentials for further reduction. Comproportionation constants that describe the equilibrium for the reaction $(IP^-)_2AlX + (IP)_2AlX \leftrightarrow (IP^-)(IP)AlX$ fall in the range of $K_c = 10^{5.7}$ to $10^{7.9}$ for **3**−**9**.

INTRODUCTION

Oxidation accompanied by a bond-forming reaction, sometimes termed a "group transfer" reaction, is an important synthetic tool often employed for access to high-valent transition metal complexes with metal−ligand multiple bonds.[1] Distinct from oxidative addition, this reaction involves oxidation of a metal complex concomitant with formation of one metal−ligand bonding interaction, which may have single or multiple bond character. The group transfer reaction is also a key elementary step in several catalytic cycles. For example, O-atom, N-group, or C-group transfer can afford an intermediate for epoxidation, aziridination, or cyclopropantion of alkenes, respectively.[2,3] Impetus to develop group transfer chemistry for the main group elements derives from two main goals. The prospect of employing the inexpensive and abundant main group elements for catalysis is appealing,[4] as is a new route to functionalization of metals that are often inert to classical substitution chemistry because of their high Lewis acidity. Because of aluminum's high natural abundance and low cost, aluminum catalysts have potential for large scale applications.[5]

As an alternative redox-mediated pathway to metal−ligand bond formation in main group systems, recent work has shown that redox-active ligands can facilitate the oxidative group transfer reaction of sulfides at redox inert metal centers. Following an oxidative group transfer pathway, the reaction of BzS−SBz with $[(dpp\text{-}Bian)Ga]_2$ afforded a Ga−S bond in the complex of $(dpp\text{-}Bian)Ga(SBz)_2$ (dpp-Bian = 1,2-bis[(2,6-diisopropylphenyl)-imino]acenapthene) in a reaction that involved one-electron oxidation of both the dpp-Bian ligand and the Ga(II) metal center.[6] We have subsequently shown that disulfides can be employed in group transfer to gallium in a two-electron oxidation reaction where both electrons originate from the redox-active iminopyridine (IP) ligand system.[7] We have also shown that pyridine-*N*-oxide (pyO) can be used as an atom transfer reagent in combination with redox active $Bu_4N[(IP^{2-})_2Al]$ (**1a**) or $[(DME)_3Na][(IP^{2-})_2Al]$ (**1b**) to afford a one-electron oxidized product $(IP^-)_2Al(OH)$ or two-

Received: May 29, 2012
Published: July 27, 2012

   dx.doi.org/10.1021/ic301128m | Inorg. Chem. 2012, 51, 8997−9004

electron oxidized product [(DME)(THF)Na][(IP^{2-})(IP^{-})Al(OH)], respectively.[8]

One potentially general route for group transfer reactions is oxidation using metal salts because a variety of groups X can be employed. This route has previously been explored to effect *one-electron* chemistry. For example, James and co-workers reported using two equivalents of a silver salt AgX to oxidize $Mo(CO)_2(bipy)_2$ to $Mo(CO)_2(bipy)_2X_2$ (where X = NO_2, NO_3, NCS).[9] Lead dihalides were shown to oxidize chromium complexes by one-electron concomitant with formation of metal halide bonds; CpCr[$(ArNCMe)_2CH$]X (where X = Cl, Br, I) was obtained.[10] Copper has also been used as a group transfer reagent; Kiplinger and co-workers employed a series of CuX salts (where X = F, Cl, Br, I, SPh, CCPh, or OTf) to oxidize U(IV) to U(V) and form new U−X bonds.[11] Because of the instability of organocuprates and copper azide reagents, transfer of acetylide and azide groups to U(IV) was approached using gold reagents in an analogous process.[12] Evans and co-workers have employed silver and copper salts in reactions that could be described as oxidative substitution rather than transfer. In these examples, methyl groups on uranium or thorium were successfully replaced by halide or triflate ligands through a redox mediated process at the metal center.[13]

Herein, we demonstrate that a general route for *two-electron* oxidative group transfer using zinc salts is efficient for formation of aluminum-X bonds; Al(III)-chloro, acetylido, azido, thiolato, and amido bonds were obtained from appropriate ZnX_2 salts. In all instances, we observed exclusively two-electron oxidized products. In tandem with the ease and scope of preparation of ZnX_2, these results suggest that ZnX_2 could find broad and predictable utility for group transfer.

RESULTS AND DISCUSSION

Syntheses of Complexes. Substitution of aluminum complexes is difficult because of the strong interaction between Lewis acidic aluminum and a coordinated ligand. Indeed, in the present work, some preliminary experiments indicated that metathesis and protonolysis are of limited utility to access a broad array of substituents in complexes of the type (IP^{-})$_2$AlX. For example, reactions of (IP^{-})$_2$AlCl (**2**)[8a] with lithium and sodium bases did not displace chloride, with the exception of MeLi, which afforded (IP^{-})$_2$Al(CH_3) (**3**) (Scheme 1). It

Scheme 1

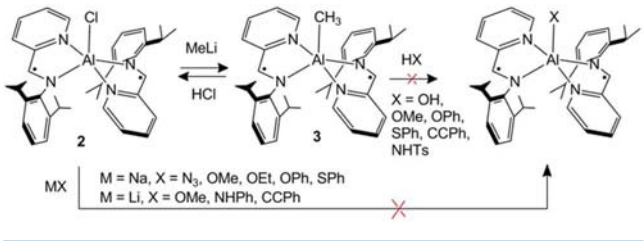

should be noted that **3** is now more readily accessed via salt metathesis of $AlCl_2Me$ and $Na_2(IP^{2-})$. Protonolysis of **3** to liberate methane was explored. Using HCl, (IP^{-})$_2$AlCl was obtained in moderate yield, but weaker acids such as alcohols, amides, anilinium, and thiol were unreactive toward **3**.

As a first step toward a more general accessibility of (IP^{-})$_2$AlX-type complexes, we extended the use of substituted disulfides to aluminum.[7] The reaction of [$(THF)_6$Na][(IP^{2-})$_2$Al] (**1c**) in THF at room temperature with tetramethylthiuram disulfide or MeSSMe gave access to (IP^{-})$_2$Al(SR) (where R = $C(S)NMe_2$, **4**; Me, **5**) (Scheme 2).

Scheme 2

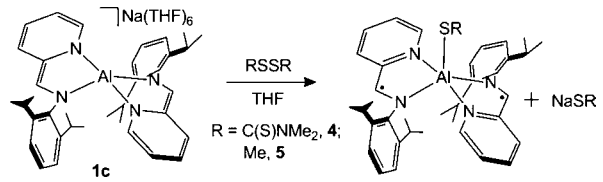

The reactions proceeded cleanly and reached completion within less than an hour to afford six-coordinate **4** and five-coordinate **5** as dark green products in good yield: 64% and 88%, respectively.

We wished to expand the observed redox reactivity of disulfides to a more general route to substitution of aluminum complexes. Accordingly, a route for aluminum−ligand bond formation via two-electron oxidation was developed on the basis of the $Zn^{2+/0}$ redox couple (Scheme 3). Zinc salts of the

Scheme 3

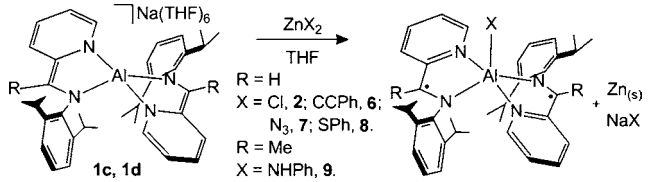

form ZnX_2 (where X = Cl, C≡CPh, N_3, SPh, or NHPh) each possess a two-electron reduction event at −1.03 ± 0.05 V vs SCE with varying degrees of reversibility. Thus, Zn^{2+} has ∼350 mV of overpotential for the oxidation of IP^{2-} to IP^{-} in complexes such as **1a** but lacks sufficient strength to access neutral IP and cause over oxidation. Oxidation of [$(THF)_6$Na][(IP^{2-})$_2$Al] (**1c**) by ZnX_2 in THF proceeded cleanly to afford complexes (IP^{-})$_2$AlX (where X = Cl, **2**; C≡CPh, **7**; N_3, **8**; and SPh, **9**), along with zinc powder and NaX that were easily separated by filtration (Scheme 3). In all cases, excess zinc salt can lead to isolation of previously reported (IP^{-})$_2$Zn,[14] but this is easily avoided.

We observed that the reaction of **1c** with protic zinc salts, such as $Zn(NHPh)_2$, yielded products that resisted crystallization attempts. To further investigate the reaction products, the green reaction solution was quenched with dilute acid to separate organic ligands from aluminum. Subsequent GC-MS analysis revealed aminopyridine. As control experiments, complexes **4**, **5**, and **6**−**8** were analyzed in an identical manner using a dilute acid quench of the reaction mixture and GC-MS analysis, and in these instances, no aminopyridine was observed. This experiment suggests that formation of aminopyridine is the result of the interaction of sufficiently acidic protons of $(HNPh)^{-}$ and the IP^{2-} moiety in **1c** or in an intermediate (IP^{-})$_2$Al(HNPh).

To afford some steric protection to the imine carbon of IP, a ligand with a methyl group in the imine carbon position was synthesized and is henceforth denoted ^{Me}IP (^{Me}IP = 2,6-bis(1-methylethyl)-*N*-(2-pyridinylethylene) phenylamine).[15] Following the same synthetic method used to make previously reported [$Na(DME)_3$][(IP^{2-})$_2$Al], the corresponding ^{Me}IP complex, [$Na(DME)_3$][($^{Me}IP^{2-}$)$_2$Al] (**1d**) was synthesized via

dx.doi.org/10.1021/ic301128m | *Inorg. Chem.* 2012, 51, 8997−9004

two-electron reduction of ^{Me}IP with sodium metal and subsequent addition of 1/2 an equivalent of $AlCl_3$. The ^{1}H NMR spectrum is consistent with the diamagnetic IP^{2-} ligand. Most notably, the dearomatized ring protons of the formerly pyridine functional group are observed at 6.73, 5.98, 5.24, and 4.52 ppm. The methyl-substitution at the imine carbon of **1d** is observed at 1.59 ppm, and the resonance at 5.53 ppm that corresponded to the imine hydrogen in **1c** is no longer apparent. The reaction of **1d** with one equivalent of $Zn(HNPh)_2$ in THF afforded the green product $(^{Me}IP^-)_2Al(NHPh)$ (**9**) in 68% (Scheme 3). Apparently, the added steric protection of the methyl substituent at the imine carbon atom was sufficient to prevent hydrogenation.

Solid-State Structures. The solid-state structures of **4**–**9** were determined from single crystals grown from chilled hexanes solutions. Crystals of **1c**, **1d**, and **3** were obtained from diffusion of pentane into THF solutions of the complexes (Figures 1–3 and Figures S1–S4 and Tables S1–S4 of the Supporting Information). We have previously reported the structure of **2**, and it is included in the discussion here for comparison with the new five-coordinate complexes.[8a] Complexes **2**, **3**, and **5**–**9** are each five coordinate with two IP^- ligands, best described as distorted trigonal pyramidal, and can be described by their τ values, which fall between 0.668 and 0.858.[16] In each complex, the two imine nitrogen atoms and the fifth monoanionic ligand occupy a trigonal plane, and the pyridine nitrogen atoms occupy the axial positions. Comparison of the complexes reveals that the amide **9** has the least deviation from an ideal trigonal bipyridamial geometry (τ = 0.858). Further inspection revealed that several other complexes also show relatively large τ values, for example, complexes **8**, **7**, and **5** have τ values of 0.813, 0.787, and 0.785, respectively. We note that these least distorted complexes, including the thiolates, **5** and **8**, azide **7**, and phenyl-substituted **9**, include the most polarizable of the ligands X that we studied. The remaining complexes with relatively less polarizable donor atoms, **2** (τ = 0.739), **6** (τ = 0.716), and **3** (τ = 0.668), display more apparent distortions from an ideal trigonal bipyramidal geometry. Complex **3** with τ = 0.668 has the largest distortion away from ideal trigonal bipyramidal geometry and contains a strongly sigma-donating methyl group. In general, there is a loose trend between the deviation from trigonal bipyramidal geometry and the hard–soft donor properties or electronegativity of the ligand, with harder, more electronegative ligands favoring more distorted geometries. We could not find evidence for an argument that would relate the steric properties of the ligands to the geometry of the complexes.

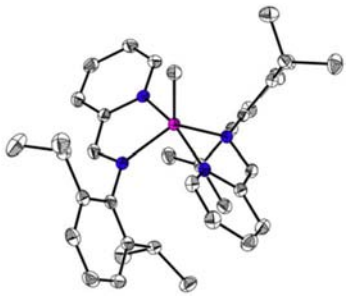

Figure 1. Solid-state structure of $(IP^-)_2Al(CH_3)$ in **3**. Pink, orange, red, blue, green, and white represent Al, Na, O, N, I, and C atoms, respectively. Ellipsoids at 40% probability. H atoms omitted.

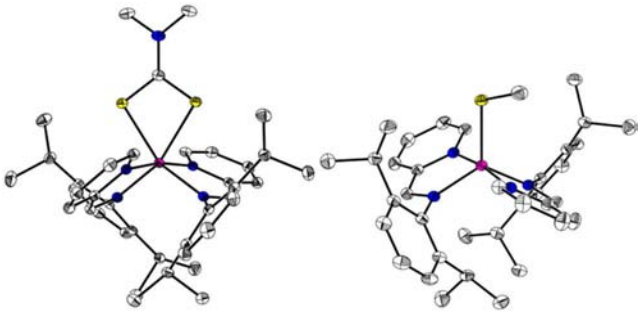

Figure 2. Solid-state structures of $(IP^-)_2Al(SC(S)NMe_2)$ in **4** and $(IP^-)_2Al(SCH_3)$ in **5**. Pink, blue, yellow and white represent Al, N, S, and C atoms respectively. Ellipsoids at 40% probability. H atoms omitted.

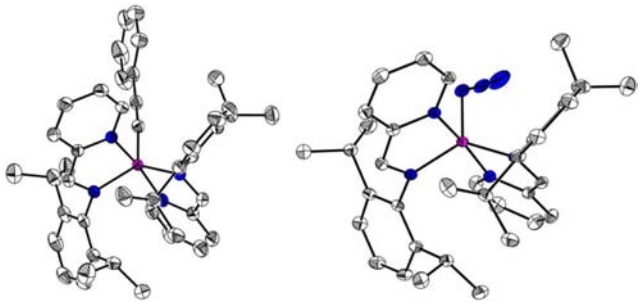

Figure 3. Solid-state structures of $(IP^-)_2Al(C{\equiv}CPh)$ in **6** and $(IP^-)_2Al(N_3)$ in **7**. Pink, blue, and white represent Al, N, and C atoms respectively. Ellipsoids at 40% probability. H atoms omitted.

The bond lengths and angles in all of the complexes **2**–**8** are consistent with the observed metrics for previously reported monoanionic IP ligands bound to main group metals.[8,15,15] The C_{im}–N_{im} bond lengths in **2**–**8** (1.345(3) to 1.396(4) Å) are roughly 0.08 Å longer than those in the neutral IP ligand (1.284(6) Å), and a contraction of the C_{im}-C_{py} bond (from 1.453(7) Å to a mean of 1.40(2) Å) accompanies this change.[8a] These observations are in agreement with the previous observations by us and others that the added electron is localized mostly at the C_{im} atom.[8a,14] Within this range of bond lengths, which can all be assigned as IP^-, we do see some variation. The longest C_{im}–N_{im} bonds were observed in amido complex **9** with a bond length of 1.396(4) Å, and **9** also has a shorter C_{im}–C_{py} bond length (1.337(6) Å) compared to that of the other complexes **2**–**8** (Figure 4). This outlying metric for **9** accompanies the outlying τ value for **9**, which as discussed earlier identifies **9** as possessing a geometry most closely approximating ideal trigonal bipyramidal of any of the complexes we have studied (Figure 4).

These observations suggested to us that **9** has the "most reduced" IP^- ligand of any that we have observed and that the degree of reduction of IP^- may be correlated with complex geometry (as represented by τ) and the polarizability/electronegativity of the X group in $(IP^-)_2AlX$. Accordingly, we were prompted to search for more general trends in the values of C_{im}–N_{im}, C_{im}–C_{py}, and τ for complexes **2**, **3**, **5**, and **6**–**9**. Indeed, complex **3** with the lowest τ value, has the "least reduced" IP^- ligand, i.e., the shortest C_{im}–N_{im} and a C_{im}–C_{py} bond length that is among the longest accounting bond length esd values. Comparison of C_{im}–N_{im} and C_{im}–C_{py} for the remaining complexes revealed that there is a trend toward shorter C_{im}–C_{py} bond length with longer C_{im}–N_{im} bond length

dx.doi.org/10.1021/ic301128m | Inorg. Chem. 2012, 51, 8997–9004

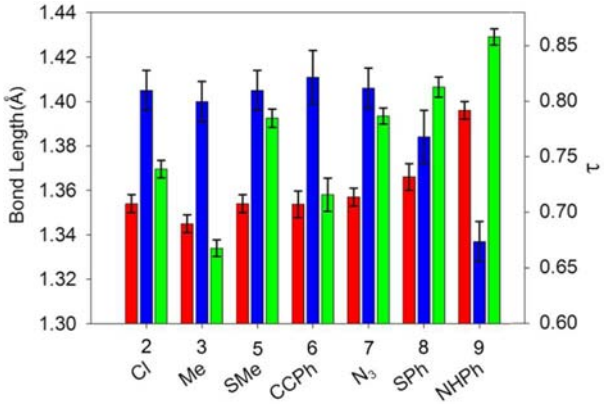

Figure 4. Histogram of the individual C_{im}–N_{im} (red) and C_{im}–C_{py} (blue) bond distances and τ (green) values in **2**, **3**, and **5**–**9**.

and smaller τ values, but that individual complexes do deviate from the trend with experimental error. Observed variations from this trend are mostly due to the small variation in C_{im}–C_{py} values, which makes any statistical or measurement uncertainties significant.

Overall, these observations imply that the more polarizable groups, such as SPh or NHPh in **8** and **9**, may accommodate the most reduced IP^- ligands and that these electronic effects are manifest in the bond lengths of the IP^- ligands and in the bond angles (as measured by the geometry parameter τ). In general, the bond distances around the pyridine ring also have slight distortions, but these are minor in comparison to the distortions in the C_{im}–C_{py} and C_{im}–N_{im} bond lengths and indicate no significant loss of aromaticity in the pyridine rings. It is also possible that the methyl substitution on the IP ligand in **9** contributes to the degree of reduction observed in $^{Me}IP^-$. We are unable to rule this out.

Electronic Structure. The electronic structure of each of the complexes **3**–**9** were probed using temperature-dependent magnetic susceptibility measurements in an applied field of 0.1 T (Figure 5, Table 1). Consistent with our previous investigations on complexes of the form $(IP^-)_2AlX$, **3**–**9** each possess biradical character at room temperature (μ_{eff} = 2.15 – 2.55 μ_B). As the temperature was lowered to 5 K, the magnetic moment of each complex fell. At 5 K, the moments all fall

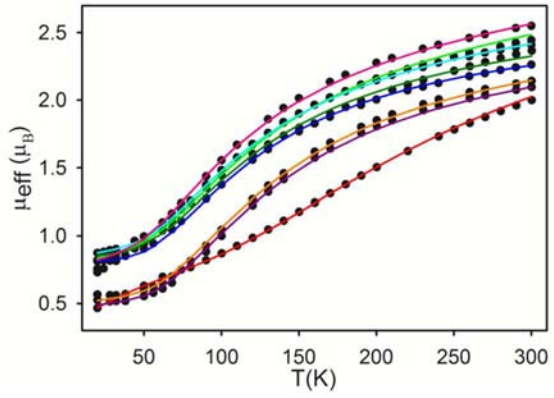

Figure 5. Magnetic susceptibility data for compounds **2** (red),[8a] **3** (orange), **4** (light green), **5** (dark green), **6** (light blue), **7** (dark blue), **8** (fuschia), and **9** (purple) in an applied field of 0.1 T. The "●" represents the experimental data, and the "—" represents a fit to the data using a spin Hamiltonian of the form $\hat{H} = -2J\hat{S}_{L(1)}\cdot\hat{S}_{L(2)}$.

Table 1. Summary of Fit Parameters for 2–9

	J (cm^{-1})	TIP (emu $\times 10^{-3}$)	paramagnetic impurity (%)
2	−212	0.750	1.1
3	−118	0.235	2.6
4	−105	0.750	6.5
5	−94	0.630	5.1
6	−99	0.530	7.6
7	−100	0.215	7.0
8	−95	0.850	6.1
9	−121	0.220	2.8

within the range 0.57–0.84 μ_B, and a fit to the data using MAGFIT 3.0,[17] assuming g = 2.0 and a spin Hamiltonian of the form $\hat{H} = -2J\hat{S}_{L(1)}\cdot\hat{S}_{L(2)}$, yielded an energy for the exchange coupling between ligand radicals of **2**–**9** ranging from J = −94 to −212 cm^{-1}. The data were fit between 20 and 300 K, considering contributions from J, TIP, and a paramagnetic impurity. Previously reported **2** was refit to include a contribution from a paramagnetic impurity, and a slightly lower value for J was obtained (212 cm^{-1}) than we had previously reported (230 cm^{-1}).[8a]

Previous work with transition metal-oxo complexes has shown that exchange coupling is often influenced by the M–O–M angular arrangement of the complex,[18] and with this in mind, the relationship between the angles between the two ligand π systems and the coupling constant J was examined. The ligand π system was defined by the plane containing N_{im}–C_{im}–C_{py}–N_{py}. In complexes **2**, **3**, and **6**–**9**, the torsion angle between these four atoms is less than 2° in all cases, indicating that the four atoms are coplanar. Using the angle between the two ligand planes (the dihedral angle) as a metric for the basis for comparison, there is indeed a correlation between the dihedral angle and the magnitude of the antiferromagnetic coupling for each of the five-coordinate complexes **2**, **3**, and **5**–**9**. The maximum energy of interaction, as represented by the magnitude of J values, occur in complexes with the smallest dihedral angle such as complexes **9** (120.25°) and **2** (118.03°)[8a] (Figures 6 and 7). Complexes with dihedral angles that are

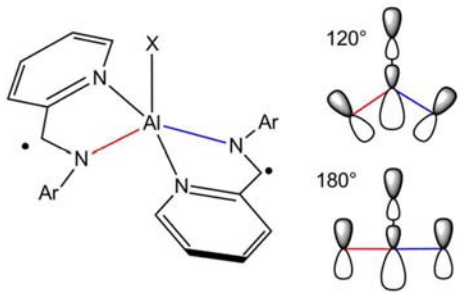

Figure 6. Possible orbital interactions in **2**, **3**, and **5**–**9** that lead to antiferromagnetic coupling.

significantly larger than 120° such as **5** (125.80°) and **8** (126.06°) show less exchange coupling, and we attribute this to a reduced interaction between IP^--based p-orbitals and a suitable orbital on the Al center; σ^* for the Al-X bond is a likely orbital (Figure 6). It is not clear to us at this stage what factors influence the magnitude of the dihedral angle. We found no correlation between the dihedral angle and any of the other structural parameters which were discussed in detail with regard

dx.doi.org/10.1021/ic301128m | Inorg. Chem. 2012, 51, 8997–9004

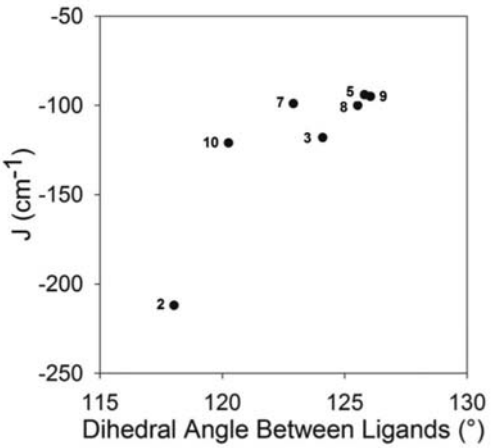

Figure 7. Plot of J (cm^{-1}) versus ligand dihedral angle between the planes defined by $N_{im}-C_{im}-C_{py}-N_{py}$ for complexes **2**, **3**, and **5**–**9**.

to the single crystal crystallographic measurements (vide supra).

Electrochemical Measurements. The electrochemical properties of **3**–**9** were investigated by cyclic voltammetry (CV) experiments performed in 0.3 M NBu_4PF_6 THF solutions. Complex **2** has been previously investigated, and we include those results here for comparison.[8a] Each CV displayed two separate one electron $IP^{0/1-}$ couples separated by between 0.34–0.47 V and located between −0.21 and −0.69 V vs SCE (Table 2, Figure 8). As discussed earlier, the bond

Table 2. Summary of Redox Events for 2–9 (V vs. SCE)

	$IP^{00/01-}$	$IP^{01-/1-1-}$	ΔE	K_c	$IP^{1-1-/1-2-}$	$1P^{2-2-/2-2-}$
2	−0.25	−0.59	0.34	$10^{5.7}$	−1.75	
3	−0.21	−0.59	0.38	$10^{6.4}$	−1.72	
4	−0.23	−0.62	0.39	$10^{6.6}$	−1.40	
5	−0.24	−0.62	0.48	$10^{6.4}$	−1.63	
6	−0.25	−0.65	0.40	$10^{6.8}$	−1.64	−1.87
7	−0.27	−0.64	0.37	$10^{6.3}$	−1.60	−1.78
8	−0.27	−0.64	0.37	$10^{6.3}$	−1.70	−1.87
9	−0.22	−0.69	0.47	$10^{7.9}$	−1.61	−1.81

metrics for **9** indicate that complex **9** has the "most reduced" IP ligand, and we observed that for each of the five-coordinate complexes, **2**, **3**, and **5**–**9**, those with longer $C_{im}-N_{im}$ bonds, i.e., those that are more reduced, have an $IP^{01-/1-1-}$ redox couple at more negative potential as would be expected for more electron-rich ligands (Figure 9, left). Complex **9** has the most negative oxidation potential, confirming it as the complex with the "most reduced" IP ligand. Again, we are unable to comment more completely on the possible effect of the methyl substituent on ^{Me}IP to the observed trends, although in Figure 9, complex **9** lies slightly off from the trend delineated by other complexes of IP^-, **2**, **3**, and **5**–**8**.

The potentials for the oxidation events, the $IP^{1-1-/1-2-}$ and $IP^{1-2-/2-2-}$ redox couples, were observed at relatively consistent locations between complexes and were observed as either a concerted two-electron process (**2**, **3**, **5**) or as consecutive one-electron processes (**6**–**9**). The average potential for the two one-electron events or the potential for the two-electron events are all centered around −1.71 V, except for in **4** where an irreversible redox couple occurs at −1.40 V. It is unclear whether this positively shifted couple should be

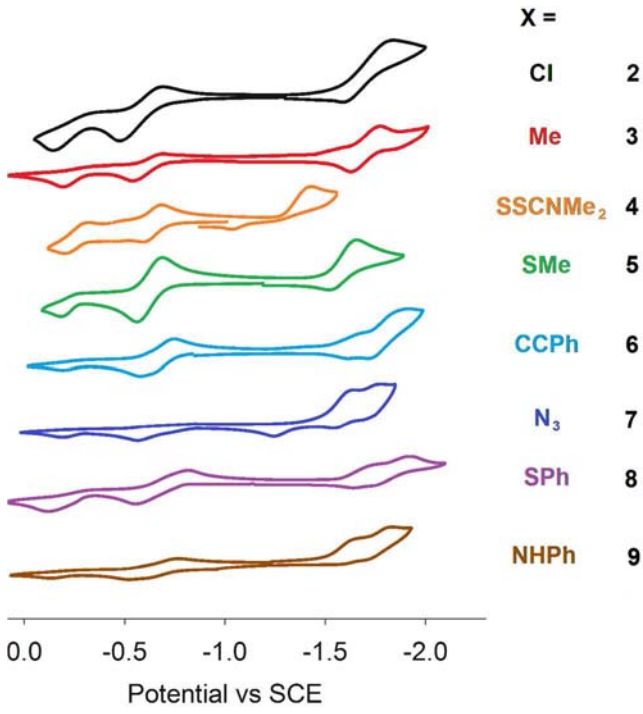

Figure 8. Cyclic voltammograms for complexes **2**–**9** in 0.3 M NBu_4PF_6 THF solution.

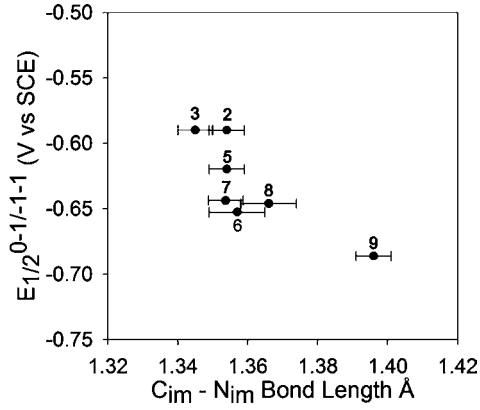

Figure 9. (Left) Plot of $E_{1/2}(IP^{01-/1-1-})$ versus $C_{im}-N_{im}$ bond distance in the five-coordinate complexes **2**, **3**, and **5**–**9**.

assigned to reduction of $SC(S)NMe_2$ or if it is indeed an IP^--based event that is anodically shifted as a result of the unusual six-coordinate Al(III) geometry of **4**. Overall, the minimal changes in the location of redox potentials upon substitution of the X ligand in $(IP^-)_2AlX$ complexes stand in stark contrast to significant shifts in the potentials of metal-centered redox events that generally occur upon ligand substitution. It should be noted that we have previously indicated that removing the X ligand from $(IP^-)_2AlX$ entirely has been shown to lower the potentials of the $IP^{-1/-2}$ by approximately 400 mV.[8a]

The values of $\Delta E_{1/2}$ for the $IP^{00/0-1}$ and $IP^{0-1/-1-1}$ couple were tabulated as K_c values for the reaction $(IP^-)_2AlX + (IP)_2AlX \leftrightarrow (IP^-)(IP)AlX$, and fell between $10^{5.7}$ for **2** and $10^{7.9}$ for **9** (Table 2). The values for K_c were compared with J values for the complexes because both should be related to the degree of orbital overlap between the two ligands and the appropriate aluminum-based orbital, possible Al-X σ^* as previously discussed. A plot of J versus $\Delta E_{1/2}$ (Figure S5 of

dx.doi.org/10.1021/ic301128m | Inorg. Chem. 2012, 51, 8997–9004

the Supporting Information, left) shows a weak correlation between these parameters. The weak correlation may be due in part to the small variation in the K_c and the small variation in J. A correlation was also observed between $\Delta E_{1/2}$ and the dihedral angle between ligand planes (Figure S5 of the Supporting Information, right)

CONCLUSION AND OUTLOOK

We have demonstrated that zinc salts, ZnX_2, are a versatile two-electron atom transfer reagent for functionalization of Al(III) complexes via a two-electron oxidative group transfer pathway. Oxidation of $[(IP^{2-})_2Al]^-$ with various ZnX_2 salts affords complexes of the form $(IP^-)_2AlX$ (where X = Cl, C≡CPh, N_3, SPh, or NHPh). The consistent potential of the $Zn^{0/2+}$ redox couple combined with the ease of preparation of the zinc salts, the wide range of compatible X groups, and the preference for two-electron chemistry makes zinc salts ideal two-electron oxidative group transfer reagents. We have shown that the resulting complexes have geometric parameters such as bond lengths and angles that are dependent on the polarizability of the X group. Specifically, these parameters suggest that more polarizable X groups support the "most reduced" IP^- ligands according to bond length data and that the less polarizable X groups are supported by complexes containing "least reduced" IP^- ligands.

The electronic structure properties of each of the complexes **2**–**9** were also thoroughly investigated. The magnitude of the magnetic exchange between ligand-based radicals is antiferromagnetic in nature and was demonstrated to be dependent on the dihedral angle between the $N_{im}-C_{im}-C_{py}-N_{py}$ ligand planes. We speculated that a smaller dihedral angle provides better overlap between p-orbitals in the π system of IP^- and the Al-X σ^* orbital as a pathway for superexchange. The electronic coupling between ligands was interrogated by cyclic voltammetry measurements, and we found that these measurements corroborated our crystallographically determined assignments of **9** as the "most reduced" IP^- ligand and **5** as the "least reduced" IP^- ligand, with other complexes falling between these extremes according to the degree of polarizability/electronegativity of the X ligand in $(IP^-)_2AlX$.

In future work, we will probe more directly the electronic structure of these complexes using DFT calculations, and we will focus on the interactions of these Al(III) complexes with small molecules, including electron transfer reactions mediated by redox active Al(III) complexes.

EXPERIMENTAL SECTION

Physical Measurements. Elemental analyses were performed by Columbia Analytical. ^{1}H NMR spectra were recorded at ambient temperature using a Varian 400 MHz spectrometer. Chemical shifts were referenced to residual solvent. Electrochemical measurements were recorded in a glovebox under a dinitrogen atmosphere using a CHI Electrochemical Analyzer, a glassy carbon working electrode, a Pt wire auxiliary-electrode, and an $Ag/AgNO_3$ nonaqueous reference electrode. Reported potentials are all referenced to the SCE couple and were determined using decamethylferrocene as an internal standard. The number of electrons passed in a given redox process was estimated by comparison of the peak current with the peak current of decamethylferrocene included as an internal standard. UV–vis spectra were recorded in THF solutions using a Varian Cary 1 UV–vis spectrometer. Magnetic measurements were recorded using a Quantum Designs MPMS XL magnetometer at 0.1 T. The sample was contained under nitrogen in a gelcap and suspended in the magnetometer in a plastic straw. The magnetic susceptibility was adjusted for diamagnetic contributions using Pascal's constants.

X-ray Structure Determinations. X-ray diffraction studies were carried out on a Bruker SMART 1000, a Bruker SMART APEXII, or a Bruker SMART APEX Duo diffractometer equipped with a CCD detector.[19a] Measurements were carried out at −175 °C using Mo Kα 0.71073 Å and Cu Kα 1.5418 Å radiation. Crystals were mounted on a glass capillary or Kaptan Loop with Paratone-N oil. Initial lattice parameters were obtained from a least-squares analysis of more than 100 centered reflections; these parameters were later refined against all data. Data were integrated and corrected for Lorentz polarization effects using SAINT[19b] and were corrected for absorption effects using SADABS2.3.[19c]

Space group assignments were based upon systematic absences, E statistics, and successful refinement of the structures. Structures were solved by direct methods with the aid of successive difference Fourier maps and were refined against all data using the SHELXTL 5.0 software package.[19d] Thermal parameters for all non-hydrogen atoms were refined anisotropically. Hydrogen atoms, where added, were assigned to ideal positions and refined using a riding model with an isotropic thermal parameter 1.2 times that of the attached carbon atom (1.5 times for methyl hydrogens).

Preparation of Compounds. All manipulations were carried out using standard Schlenk or glovebox techniques under a dinitrogen atmosphere. Unless otherwise noted, solvents were deoxygenated and dried by thorough sparging with Ar gas followed by passage through an activated alumina column. Deuterated solvents were purchased from Cambridge Isotopes Laboratories, Inc. and were degassed and stored over activated 3 Å molecular sieves prior to use. The compounds 2,6-bis(1-methylethyl)-*N*-(2-pyridinylmethylene)-phenylamine[15] (abbreviated as IP), 2,6-bis(1-methylethyl)-*N*-(2-pyridinylethylene) phenylamine (abbreviated as ^{Me}IP),[20] $(IP^-)_2AlCl$,[8a] $(Bu_4N)[(IP^{2-})_2Al]$ (**1a**),[8a] $[(Et_2O)_2Na][(IP^{2-})Al]$ (**1b**),[8b] $Zn(C{\equiv}CPh)_2(py)_2$,[21] $Zn(N_3)_2(py)_2$,[22] $Zn(SPh)_2(py)_2$,[23] and $Zn(NHPh)_2(py)_2$[24] were prepared according to literature procedures. All other reagents were purchased from commercial vendors and used without further purification.

$[Na(THF)_6][(IP^{2-})_2Al]$ (1c). (731 mg, 1.0 mmol) was stirred in 10 mL of THF, and then the solution was concentrated to 2 and 10 mL of hexanes was layered on top. After the solution cooled at −25 °C overnight, **1c** (940 mg, 93%) was obtained as a dark pink solid. Crystals suitable for X-ray diffraction were grown by slow diffusion of pentane into a concentrated THF solution at −25 °C. ^{1}H NMR (400 MHz, C_6D_6): δ 7.25 (t, J = 6.15, 2H, Ph), 7.11 (d, J = 6.55, 2H, Ph), 6.79 (d, J = 6.01, 2H, Ph), 5.88 (d, J = 8.79, 2H, py), 5.53 (s, 2H, imC*H*), 5.28 (dd, J = 8.63, 5.04, 2H, py), 4.66 (t, J = 9.05, 2H, py), 4.14 (hept, J = 6.7, 2H, C*H*$(CH_3)_2$), 3.44 (br, 24H, THF), 1.45 (d, J = 7.13, 6H, CH(C*H*$_3)_2$), 1.36 (d, J = 6.11, 6H, CH(C*H*$_3)_2$), 1.22 (br, 24H, THF). IR(cm^{-1}): 1573 (s, im^{2-}). Anal. Calcd for $C_{60}H_{92}AlN_4NaO_6$: C, 70.97; H, 9.13; N, 5.52. Found: C, 71.11; H, 8.97; N, 5.44. UV–vis spectrum (THF) λ_{max} (ε_M): 286 (21 550), 447 (4320) nm (L $mol^{-1}cm^{-1}$). This compound is diamagnetic.

$[Na(DME)_3][(^{Me}IP^{2-})_2Al]$ (1d). Sodium metal (242 mg, 10.5 mmol) and ^{Me}IP (1.40 g, 5.0 mmol) were stirred in DME (10 mL) for 1 h. The resulting deep red solution was added to a stirred suspension of $AlCl_3$ (333 mg, 2.5 mmol) in DME (10 mL), and the mixture was stirred for 24 h to afford a deep purple suspension. The solvent was removed in vacuo, and the purple solid was extracted into ether (4 × 20 mL) and filtered through Celite. The solution was concentrated to 10 mL and cooled at −25 °C overnight. Purple **1d** (1.83 g, 83%) was collected by filtration. Crystals suitable for xray diffraction were grown by cooling a concentrated ether solution at −25 °C for 3 days. ^{1}H NMR (400 MHz, C_6D_6): δ 7.25 (t, J = 7.15, 2H, Ph), 7.09 (d, J = 7.25, 2H, Ph), 6.73 (d, J = 6.4, 2H, py), 5.98 (d, J = 9.6, 2H, py), 5.24 (dd, J = 9.6, 6.4, 2H, py), 4.52 (t, J = 5.7, 2H, py), 4.09 (hept, J = 6.7, 2H, C*H*$(CH_3)_2$), 3.03 (br, 30H, DME), 1.77 (d, J = 6.70, 6H, CH(C*H*$_3)_2$), 1.59 (s, 6H, imC*H*$_3$), 1.42 (d, J = 6.70, 6H, CH(C*H*$_3)_2$), 1.25 (d, J = 6.70, 6H, CH(C*H*$_3)_2$), 0.42 (d, J = 6.70, 6H, CH(C*H*$_3)_2$). IR(cm^{-1}): 1575 (s, im^{2-}). Anal. Calcd for $C_{48}H_{74}AlN_4NaO_6$: C, 68.15; H, 8.92; N, 6.36. Found: C, 68.44; H, 9.13; N, 6.44. UV–vis spectrum (THF) λ_{max}

dx.doi.org/10.1021/ic301128m | Inorg. Chem. 2012, 51, 8997–9004

(ε_M): 290 (24 330), 445 (4440) nm (L mol^{-1}cm^{-1}). This compound is diamagnetic.

(IP$^-$)$_2$AlCl (2). To a stirred solution of **1c** (1.01 g, 1.0 mmol) in THF (10 mL) was added $ZnCl_2$ (134 mg, 1.0 mmol). The resulting solution was stirred for 1 h after which the green solution was evaporated to dryness. The crude product was extracted into hexanes (20 mL) and filtered through Celite to remove zinc metal and salts. The filtrate was concentrated to 10 mL and allowed to cool at −25 °C for 2 days. Formation of dark green **5** (460 mg, 77%) was confirmed by comparison of unit cells to previously obtained crystals.[8a]

[(IP$^-$)$_2$Al(CH$_3$)] (3) Method A. A solution of methyllithium (1.4 mL, 1.9 mmol, 1.4 M ether) was added to a stirred solution of **5** (1.00 g, 1.7 mmol) dissolved in 10 mL of ether at −25 °C. The deep green solution was stirred for 16 h, and then the resulting solution was filtered through Celite to remove a white precipitate. The dark green filtrate was reduced in volume to 4 mL, and after chilling at −25 °C for one week, 690 mg (71%) of **6** was collected as dark green crystals suitable for X-ray diffraction. IR (cm^{-1}): 1587 (s, im$^-$). Anal. Calcd for $C_{37}H_{47}AlN_4$: C, 77.12; H, 8.24; N, 9.75. Found: C, 76.67; H, 8.29; N, 9.35. UV−vis spectrum (THF) λ_{max} (ε_M): 363 (20 550), 425 (4810), 458 (4190), 694 (br, 1070) nm (L mol^{-1}cm^{-1}). μ_{eff} = 2.15 μ_B.

[(IP$^-$)$_2$Al(CH$_3$)] (3) Method B. Compound **6** was alternatively prepared by stirring sodium metal (87 mg, 3.8 mmol) and IP (1.00 g, 3.8 mmol) in ether for 24 h. To this solution was added a solution of $AlCl_2Me$ (1.9 mL, 1.9 mmol, 1.0 M in hexanes). The resulting green solution was evaporated to dryness, extracted into hexanes (30 mL), and filtered through Celite. The filtrate was concentrated to 15 mL, and the resulting green solution was cooled at −25 °C overnight. Compound **6** was obtained as a dark green powder (890 mg, 82%). Crystals suitable for X-ray diffraction were obtained by cooling an ether solution of **6** at −25 °C for 1 week.

(IP$^-$)$_2$Al(μ^2-SSCN(CH$_3$)$_2$) (4). A solution of **1c** (1.01 g, 1.0 mmol) in THF (10 mL) was added to a stirred solution of dimethylthiuram disulfide (240 mg, 1.0 mmol) dissolved in 10 mL of THF. The deep green solution was stirred for 1 h and evaporated to dryness. The resulting green solid was extracted into hexane (10 mL) and filtered through Celite to remove salts. The solution was cooled at −25 °C for 2 days, and (IP$^-$)$_2$Al(μ^2-SSCNMe$_2$) was isolated as dark green crystals (435 mg, 64%). IR (cm^{-1}): 1586 (vs, im$^-$), 933 (m, C═S), 923 (m, C═S). Anal. Calcd for $C_{39}H_{50}AlN_5S_2$: C, 68.89; H, 7.41; N, 10.30. Found: C, 68.64; H, 7.46; N, 10.12. UV−vis spectrum (THF) λ_{max} (ε_M): 369 (23 730), 440 (8140), 745 (br, 2560) nm (L mol^{-1}cm^{-1}). μ_{eff} = 2.46 μ_B.

(IP$^-$)$_2$Al(SCH$_3$) (5). A solution of **1c** (1.01 g, 1.0 mmol) in THF (10 mL) was added to a stirred solution of CH_3SSCH_3 (94.0 mg, 1.0 mmol) dissolved in 10 mL of THF. The deep green solution was stirred for 1 h and evaporated to dryness. The resulting green solid was extracted into hexane (10 mL) and filtered through Celite a second time to remove salts. The solution was cooled at −25 °C for 2 days, and (IP$^-$)$_2$Al(SCH$_3$) was isolated as dark green crystals (533 mg, 88%). IR (cm^{-1}): 1584 (vs, im). Anal. Calcd for $C_{37}H_{47}AlN_4S$: C, 73.23; H, 7.81; N, 9.23. Found: C, 73.50; H, 7.65; N, 9.04. UV−vis spectrum (THF) λ_{max} (ε_M): 357 (26150), 414 (9550), 446 (8130), 668 (br, 2730) nm (L mol^{-1}cm^{-1}). μ_{eff} = 2.46 μ_B.

(IP$^-$)$_2$Al(C≡CPh) (6). A solution of **1c** (1.01 g, 1.0 mmol) in THF (10 mL) was added to a stirred solution of Zn(C≡CPh)$_2$(py)$_2$ (424 mg, 1.0 mmol) dissolved in 10 mL of THF. The deep green solution was stirred for 1 h and then filtered through Celite to remove a gray precipitate. The THF was removed under vacuum, and the resulting green solid was extracted into hexane (10 mL) and filtered through Celite a second time to remove brown impurities. The solution was cooled at −25 °C for 2 days, and (IP$^-$)$_2$Al(C≡CPh) was isolated as dark green crystals (482 mg, 73%). IR (cm^{-1}): 2121 (m, C≡C), 1591 (vs, im). Anal. Calcd for $C_{44}H_{49}AlN_4$: C, 79.97; H, 7.47; N, 8.48. Found: C, 80.05; H, 7.53; N, 8.24. UV−vis spectrum (THF) λ_{max} (ε_M): 365 (23 280), 430 (6110), 460 (5240), 691 (br, 2070) nm (L mol^{-1}cm^{-1}). μ_{eff} = 2.42 μ_B.

(IP$^-$)$_2$Al(N$_3$) (7). A solution of **1c** (1.01 g, 1.0 mmol) in THF (10 mL) was added to a stirred solution of Zn(N$_3$)$_2$(py)$_2$ (306 mg, 1.0 mmol) dissolved in 10 mL of THF. The deep green solution was stirred for 1 h, and then the resulting solution was filtered through Celite to remove a gray precipitate. The solvent was removed under vacuum, and the resulting green solid was extracted into hexane (10 mL) and filtered through Celite a second time to remove salts. The solution was cooled at −25 °C for 2 days, and (IP$^-$)$_2$Al(N$_3$) was isolated as dark green crystals (469 mg, 78%). IR (cm^{-1}): 2104 (vs, N$_3$), 1589 (vs, im$^-$). Anal. Calcd for $C_{36}H_{44}AlN_7$: C, 71.85; H, 7.37; N, 16.29. Found: C, 71.79; H, 7.44; N, 16.40. UV−vis spectrum (THF) λ_{max} (ε_M): 362 (26 260), 439 (8780), 471 4540), 720 (br, 2020) nm (L mol^{-1}cm^{-1}). μ_{eff} = 2.26 μ_B.

(IP$^-$)$_2$Al(SPh) (8). A solution of **1c** (1.01 g, 1.0 mmol) in THF (10 mL) was added to a stirred solution of Zn(SPh)$_2$(py)$_2$ (440 mg, 1.0 mmol) dissolved in 10 mL of THF. The deep green solution was stirred for 1 h, and then the resulting solution was filtered through Celite to remove a gray precipitate. The solvent was removed under vacuum, and the resulting green solid was extracted into hexane (10 mL) and filtered through Celite a second time to remove brown impurities. The solution was cooled at −25 °C for 2 days, and (IP$^-$)$_2$Al(SPh) was isolated as dark green crystals (388 mg, 58%). IR (cm^{-1}): 1588 (vs, im$^-$). Anal. Calcd for $C_{42}H_{49}AlN_4S$: C, 75.41; H, 7.38; N, 8.38. Found: C, 75.32; H, 7.52; N, 8.12. UV−vis spectrum (THF) λ_{max} (ε_M): 371 (22 230), 441 (9110), 468 (7260), 741 (br, 2060) nm (L mol^{-1}cm^{-1}). μ_{eff} = 2.55 μ_B.

(^{Me}IP$^-$)$_2$Al(NHPh) (9). A solution of **1d** (880 mg, 1 mmol) in THF (10 mL) was added to a stirred solution of Zn(NHPh)$_2$(py)$_2$ (407 mg, 1.0 mmol) dissolved in 10 mL of THF. The deep green solution was stirred for 1 h, and then the resulting solution was filtered through Celite to remove a gray precipitate. The solvent was removed under vacuum, and the resulting green solid extracted into hexane (10 mL) and filtered through Celite a second time to remove salts. The solution was cooled at −25 °C for 2 days and **9** was isolated as dark green crystals (462 mg, 68%). IR (cm^{-1}): 3347 (m, NH), 1590 (vs, im$^-$). Anal. Calcd for $C_{42}H_{50}AlN_5$: C, 77.73; H, 8.01; N, 10.3. Found: C, 78.24; H, 8.42; N, 10.16. UV−vis spectrum (THF) λ_{max} (ε_M): 360 (22 620), 443 (9430), 470 4050), 712 (br, 2320) nm (L mol^{-1}cm^{-1}). μ_{eff} = 2.18 μ_B.

■ ASSOCIATED CONTENT

Ⓢ Supporting Information

CIF files, crystal structures, plot of J vs $\Delta E_{1/2}$. This material is available free of charge via the Internet at http://pubs.acs.org.

■ AUTHOR INFORMATION

Corresponding Author

*E-mail: laberben@ucdavis.edu.

Notes

The authors declare no competing financial interest.

■ ACKNOWLEDGMENTS

We thank the University of California Davis for support of this work and the National Science Foundation (Grant 0840444) for the Dual source X-ray diffractometer. We thank Drs. M. Shanmugam and J. C. Fettinger, and G. M. Yee for experimental assistance.

■ REFERENCES

(1) Gunay, A.; Theopold, K. H. *Chem. Rev.* **2010**, *110*, 1060.

(2) (a) Müller, P.; Fruit, C. *Chem. Rev.* **2003**, *103*, 2905. (b) Wicker, B. F.; Scott, J.; Fout, A. R.; Pink, M.; Mindiola, D. J. *Organometallics* **2011**, *30*, 2453.

(3) (a) Hamaker, C. G.; Mirafzal, G. A.; Woo, L. K. *Organometallics* **2001**, *20*, 5171. (b) Li, Y.; Huang, J. S.; Che, C. M.; You, X. Z. *J. Am. Chem. Soc.* **2002**, *124*, 13185.

(4) (a) Power, P. P.; Gabbaï, F. P. *Inorg. Chem.* **2011**, *50*, 12221. (b) Jeong, J. U.; Tao, B.; Sagasser, I.; Henniges, H.; Sharpless, K. B. *J. Am. Chem. Soc.* **1998**, *120*, 6844. (c) Stephan, D. W. *Org. Biomol. Chem.* **2008**, *6*, 1535.

(5) (a) Atwood, D. W.; Yearwood, B. C. *J. Organomet. Chem.* **2000**, *600*, 186. (b) Suyama, K.; Sakai, Y.; Matsumoto, K.; Saito, B.; Katsuki, T. *Angew. Chem.* **2010**, *122*, 809. (c) Oooi, T.; Miura, T.; Maruoka, K. *Angew. Chem., Int. Ed.* **1998**, *37*, 2347.
(6) Fedushkin, I. L.; Nikipelov, A. S.; Skatova, A. A.; Maslova, O. V.; Lukoyanov, A. N.; Fukin, G. K.; Cherkasov, A. V. *Eur. J. Inorg. Chem.* **2009**, 3742.
(7) Kowolik, K.; Shanmugam, M.; Myers, T. W.; Cates, C. D.; Berben, L. A. *Dalton Trans* **2012**, Advance Article.
(8) (a) Myers, T. W.; Kazem, N.; Stoll, S.; Britt, R. D.; Shanmugam, M.; Berben, L. A. *J. Am. Chem. Soc.* **2011**, *133*, 8662. (b) Myers, T. W.; Berben, L. A. *J. Am. Chem. Soc.* **2011**, *133*, 11865.
(9) Connor, J. A.; James, E. J. *J. Organomet. Chem.* **1985**, 301.
(10) Smith, K. M *Organometallics* **2005**, *24*, 778 , Cp = cyclopentadienyl, $(ArNCMe)_2$ = β-diketiminate..
(11) (a) Graves, C. R.; Scott, B. L.; Morris, D. E.; Kiplinger, J. L. *Organometallics* **2008**, *27*, 3335. (b) Graves, C. R.; Vaughn, A. E.; Schelter, E. J.; Thompson, J. D.; Morris, D. E.; Kiplinger, J. L. *Inorg. Chem.* **2008**, *47*, 11879. (c) Graves, C. R.; Scott, B. L.; Morris, D. E.; Kiplinger, J. L. *J. Am. Chem. Soc.* **2007**, *39*, 11914.
(12) Thomson, R. K.; Graves, C. R.; Scott, B. L.; Kiplinger, J. L. *Eur. J. Inog. Chem.* **2009**, 1451.
(13) Evans, W. J.; Walensky, J. R.; Ziller, J. W. *Organometallics* **2010**, *29*, 101.
(14) Lu, C. C.; Bill, E.; Weyhermüller, T.; Bothe, E.; Wieghardt, K. *J. Am. Chem. Soc.* **2008**, *130*, 3181.
(15) Laine, T. V.; Klinga, M.; Leskelä, M. *Eur. J. Inorg. Chem.* **1999**, 959.
(16) Addison, A. W.; Rao, T. N.; Van Rijn, J. J.; Verschoor, G. C. *J. Chem. Soc., Dalton Trans.* **1984**, 1349.
(17) Schmitt, E. A. Ph. D. Thesis, University of Illinois Urbana-Champaign, Urbana, IL. 1995.
(18) Weihe, H.; Güdel, H. U. *J. Am. Chem. Soc.* **1998**, *120*, 2870.
(19) (a) *SMART Software Users Guide*, Version 5.1; Bruker Analytical X-Ray Systems, Inc.; Madison, WI, 1999. (b) *SAINT Software Users Guide*, Version 7.0; Bruker Analytical X-Ray Systems, Inc.; Madison, WI, 1999. (c) Sheldrick, G. M. *SADABS*, Version 2.03; Bruker Analytical X-Ray Systems, Inc.; Madison, WI, 2000. (d) Sheldrick, G. M. SHELXTL Version 6.12, Bruker Analytical X-Ray Systems, Inc.; Madison, WI, 1999. (e) *International Tables for X-Ray Crystallography*; Kluwer Academic Publishers: Dordrecht, 1992; Vol. *C*.
(20) Meneghetti, S. P.; Lutz, P. J.; Kress, J. *Organometallics* **1999**, *18*, 2734.
(21) Clegg, W.; García-Álvarez, J.; García-Álvarez, P.; Graham, D. V.; Harrington, R. W.; Hevia, E.; Kennedy, A. R.; Mulvey, R. E.; Russo, L. *Organometallics* **2008**, *27*, 2654.
(22) Viaud, M. C.; Rollin, P. *Synthesis* **1989**, 130.
(23) Anjali, K. S.; Sampanthar, J. T.; Vittal, J. J. *Inorg. Chim. Act.* **1999**, *295*, 9.
(24) Rees, W. S., Jr; Green, D. M.; Hesse, W. *Polyhedron* **1992**, *11*, 1697.